A NONPARAMETRIC RECONSTRUCTION AND ITS MATRIX IMPLEMENTATION FOR THE DIFFUSION ORIENTATION TRANSFORM (DOT)

Evren Özarslan[1,2], *Timothy M. Shepherd*[3], *Baba C. Vemuri*[2], *Stephen J. Blackband*[3], *Thomas H. Mareci*[4]

[1]STBB / LIMB / NICHD / NIH, Bethesda, MD, USA.
[2]Dept. of Computer & Information Science & Engineering, [3]Dept. of Neuroscience,
[4]Dept. of Biochemistry & Molecular Biology, Gainesville, FL, USA.

ABSTRACT

The diffusion orientation transform (DOT) enables the computation of orientational probability profiles from high angular resolution diffusion-weighted magnetic resonance imaging data, making it possible to map connectivity information even in regions with complex microstructure. The initial formulation of the DOT has yielded probabilities in terms of spherical harmonics. In this paper, an alternative reconstruction method is introduced that makes it possible to directly compute the probabilities. The proposed reconstruction effectively combines the reconstruction and surface estimation steps in the visualization of the probability profiles. A matrix formulation is proposed that simplifies the implementation of the DOT method. The simulation as well as experimental results demonstrate the accuracy and robustness of the approach.

1. INTRODUCTION

Since its inception, diffusion tensor imaging (DTI) [1, 2] has been the most popular systematic method used to characterize the diffusional anisotropy observed in multiorientational diffusion-weighted MRI scans. DTI has enabled the simple estimation of fiber directions as well as quantitative measures of anisotropy. Although DTI has been quite successful in achieving these goals in environments with single dominant orientation, it is incapable of resolving distinct fiber orientations in regions with more complicated structure.

In general, the diffusional attenuation of MR signal ($E(\mathbf{q})$) in pulsed field gradient experiments [3] is related to the ensemble averaged water displacement probabilities $P(\mathbf{R})$ through a Fourier integral [4]

$$P(\mathbf{R}) = \int E(\mathbf{q}) \exp(-2\pi i \mathbf{q} \cdot \mathbf{R}) \, d\mathbf{q} \, , \qquad (1)$$

where $\mathbf{R}$ is the displacement vector and $\mathbf{q}$ is the reciprocal space vector defined by $\mathbf{q} = \gamma \delta \mathbf{G}/2\pi$, where γ is the gyromagnetic ratio and $\mathbf{G}$ is the gradient vector. This equation is

exact when the narrow pulse condition is met, i.e. when the duration of the applied diffusion sensitizing gradients (δ) is much smaller than the time between the two pulses (Δ).

Diffusional anisotropy is well-reflected in the water displacement probabilities that can be obtained from Eq. 1 and it is expected that in fibrous tissues, the orientations specified by large displacement probabilities will coincide with the fiber orientations. However, direct application of Eq. 1, such as using a fast Fourier transform (FFT), would necessitate too many MRI scans (hence long acquisition times) some of which with very high magnetic field gradients. These factors are undesirable in clinical environments [5].

A high angular resolution diffusion imaging (HARDI) method [6] was introduced that samples only one spherical shell in q-space (in addition to a single acquisition at $q \approx 0$). Because of this, HARDI method allows the detection of orientational complexity with relatively small number of acquisitions without the need to apply very strong gradients. However, a major challenge in HARDI is transforming the signal values into an acceptable estimate of probability values. The *Diffusion Orientation Transform* (DOT) [7] was recently introduced that describes how this transformation can be done. In the next section we briefly review the DOT technique. In section 3, we introduce an alternative formulation of the method that enables the direct estimation of the probability values and a matrix formulation of the same. Some validation and experimental results are demonstrated in Section 4. We conclude the paper with a brief discussion in Section 5.

2. THE DIFFUSION ORIENTATION TRANSFORM

Eq. 1 can be written in spherical coordinates using the Rayleigh expansion for plane waves [8]

$$e^{\pm 2\pi i \mathbf{q} \cdot \mathbf{R}} = 4\pi \sum_{l=0}^{\infty} \sum_{m=-l}^{l} (\pm i)^l j_l(2\pi q r) \, Y_{lm}(\mathbf{u})^* \, Y_{lm}(\mathbf{r}) \, , \qquad (2)$$

where $j_l(2\pi q r)$ and $Y_{lm}(\mathbf{u})$ are the spherical Bessel functions and spherical harmonics respectively, $q = |\mathbf{q}|$, $\mathbf{u} = \mathbf{q}/q$ and similarly $r = |\mathbf{R}|$, $\mathbf{r} = \mathbf{R}/r$. The resulting three dimensional

integral can be separated into its radial and angular parts. The radial integral can be evaluated analytically and for a particular value $r = R_0$, it is given by

$$I_l(\mathbf{u}) = A_l(\mathbf{u}) \frac{\exp(-\beta(\mathbf{u})^2/4)}{(4\pi D(\mathbf{u})t)^{3/2}} + B_l(\mathbf{u}) \frac{\operatorname{erf}(\beta(\mathbf{u})/2)}{4\pi R_0^3} , \quad (3)$$

where $A_l(\mathbf{u})$, $B_l(\mathbf{u})$ and $\beta(\mathbf{u})$ are defined in the Appendix. In the above derivation it was assumed that the signal attenuation is given by

$$E(\mathbf{q}) = \exp(-4\pi^2 q^2 t D(\mathbf{u})) , \quad (4)$$

where $t = \Delta - \delta/3$ and $D(\mathbf{u})$ is the apparent diffusivity profile.

This procedure makes it possible to express the probability of water molecules to move a distance R_0 along different directions $\mathbf{r}$ in terms of a spherical tensor, i.e.

$$P(R_0\mathbf{r}) = \sum_{l=0}^{\infty} \sum_{m=-l}^{l} p_{lm} Y_{lm}(\mathbf{r}) , \quad (5)$$

where the components of this spherial tensor are given by

$$p_{lm} = (-1)^{l/2} \int d\mathbf{u} \, Y_{lm}(\mathbf{u})^* I_l(\mathbf{u}) . \quad (6)$$

Therefore, a probability profile can be computed from Eq. 5 by taking the l-th order spherical harmonic transform of the functions $I_l(\mathbf{u})$.

3. NONPARAMETRIC RECONSTRUCTION

An alternative form of the Rayleigh expansion in Eq. 2 is given by

$$e^{\pm 2\pi i \mathbf{q} \cdot \mathbf{R}} = \sum_{l=0}^{\infty} (\pm i)^l (2l+1) j_l(2\pi q r) P_l(\mathbf{u} \cdot \mathbf{r}) , \quad (7)$$

which is just a consequence of the addition theorem for spherical harmonics [8]. In Eq. 7, P_l is the l-th order Legendre polynomial. Employing this form of the Rayleigh expansion in our formalism does not change the radial integral and the probability values are given by

$$
\begin{aligned}
P(R_0\mathbf{r}) &= \frac{1}{4\pi} \sum_{l=0}^{\infty} (-i)^l (2l+1) \int d\mathbf{u} \, I_l(\mathbf{u}) P_l(\mathbf{u} \cdot \mathbf{r}) \\
&= \sum_{l=0}^{\infty} \int d\mathbf{u} \, (-1)^{l/2} \frac{2l+1}{4\pi} P_l(\mathbf{u} \cdot \mathbf{r}) I_l(\mathbf{u}) ,
\end{aligned}
\quad (8)
$$

with the definition of I_l as in Eq. 3.

The above expression provides an alternate estimation of the results that could be obtained from the parametric reconstruction. The schematic description of the nonparametric reconstruction is given by

$$D(\mathbf{u}) \xrightarrow{\text{Eq.3}} I_l(\mathbf{u}) \xrightarrow{\text{Eq.8}} P(R_0\mathbf{r}) \quad (9)$$

3.1. A Matrix Implementation

It is possible to express the above formulation in matrix form. Suppose that the HARDI experiment is performed with the application of diffusion sensitizing gradients along N_G directions. Let the direction describing the j-th gradient be denoted by the unit vector $\mathbf{u}_j$. Similarly, the unit vector describing the i-th direction along which the probability will be estimated shall be represented with $\mathbf{r}_i$, where the total number of such directions is N_R. Then Eq. 8 can be expressed simply by

$$\mathbf{T} = \sum_{l=0}^{\infty} \mathbf{M}_l \mathbf{Z}_l , \quad (10)$$

where $\mathbf{T}$ is the N_R-dimensional vector of probabilities. In Eq. 10, the components of the N_G-dimensional vector $\mathbf{Z}_l$ are given by

$$(\mathbf{Z}_l)_j = I_l(\mathbf{u}_j) , \quad (11)$$

and the components of the $N_R \times N_G$-dimensional matrix $\mathbf{M}_l$ are given by

$$(\mathbf{M}_l)_{ij} = \frac{w_j}{4\pi} (-1)^{l/2} (2l+1) P_l(\mathbf{u}_j \cdot \mathbf{r}_i) , \quad (12)$$

where w_j are the integration weights associated with each of the gradient directions computed from the areas of the Voronoi cells around each of the sample points on the unit sphere. It is important to note that the matrices $\mathbf{M}_l$ can be computed once for each gradient sampling scheme. Therefore, the only computational burden is due to the pixel-by-pixel estimation of $I_l(\mathbf{u}_j)$ (which is a straightforward operation) and the matrix multiplications given in Eq. 10. Furthermore, since $P_0(x) = 1$, all rows of the matrix $\mathbf{M}_0$ are identical. Therefore, for $l = 0$ one does not have to perform a matrix multiplication. Additionally, all terms arising from the odd values of l vanish as a consequence of the antipodal symmetry of the problem. Therefore, the total number of required matrix multiplications is only $l_{\max}/2$, when the series in Eq. 8 is terminated at $l = l_{\max}$.

The parametric resronstuction enables one to express the probabilities in terms of a Laplace series, whereas the nonparametric reconstruction made it possible to directly estimate the probability values. It is simpler to implement the latter scheme since it is unnecessary to compute a spherical harmonic transform. However, when the Laplace series in Eq. 5 is terminated at $l = l_{\max}$, and upon employing the parametric reconstruction, it was possible to express the probability values in terms of $(l_{\max} + 1)(l_{\max} + 2)/2$ numbers, which is typically much smaller than the number of directions along which the probabilities are estimated (N_R) when one visualizes the probability surfaces. This enables more efficient storage of the probability profiles in computer memory when parametric reconstruction is performed.
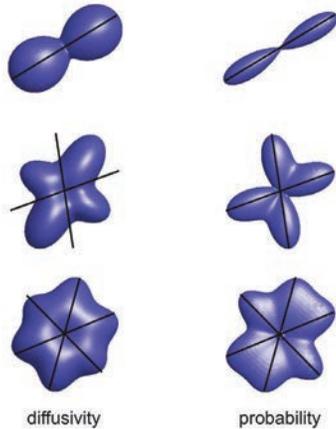
Fig. 1. Apparent diffusivity (left column) and displacement probability (right column) profiles obtained using the DOT, calculated from simulations of 1, 2 and 3 fiber systems (top to bottom). Black lines depict the exact orientations of the simulated fibers. All fibers lie on the image plane. Note that the peaks of the diffusivity profiles do not necessarily yield the orientations of the distinct fiber populations—hence the need to transform the diffusivities into probability profiles.

4. RESULTS

We have performed simulations of 1, 2 and 3-fiber voxels by employing the exact form of the MR signal attenuation from particles diffusing inside cylindrical boundaries [9] with parameters provided in [10]. We have computed the probability profiles from fiber configurations whose fiber orientations are specified by the azimuthal angles $\phi_1 = 30°$, $\phi_2 = \{20°, 100°\}$ and $\phi_3 = \{20°, 75°, 135°\}$ for the 1, 2 and 3 fiber systems respectively. Polar angles for all fibers were taken to be $90°$ so that a view from the $+z$-axis will clearly depict the individual fiber orientations. The results are shown in Figure 1. Computations with other polar angles yielded similar quality results. In all computations, the series were terminated at $l = 8$.

To provide a more quantitative assessment of the DOT method and its sensitivity to increasing noise levels, we took the HARDI simulations of 1, 2 and 3 fiber profiles presented in Figure 1 and numerically computed the fiber orientations by finding the maxima of the probability profiles (see Table 1). In this table, ψ denotes the angle between the computed and the true fiber orientations in degrees whereas σ is the noise level added to the complex signal values in quadrature. Note that when no noise was introduced ($\sigma = 0$), there was a small deviation of the computed fiber direction from the true fiber orientation because of the finite sampling of the hemisphere (at 81 gradient orientations), the termination of the series at order 8 and the precision of the numerical pro-
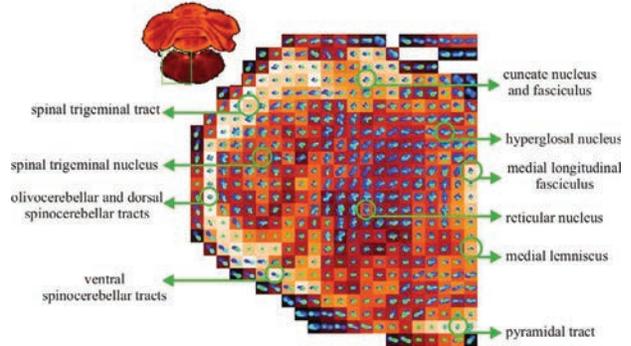
Fig. 2. The Diffusion Orientation Transform (DOT) described in this paper characterized the complex cytoarchitecture of the rat brainstem well as shown in this probability map from one side of the rat medulla.

cedure used to compute the maxima of the probability profiles. The simulations of the signal profiles with noise were repeated 100 times for each noise level to provide a distribution of deviation angles. We report the mean and standard deviations of these distributions in columns 3-6 of Table 1. As expected, the ψ values increase with increasing noise and it is more challenging to accurately resolve the distinct fiber orientations when there are more fiber orientations.

In order to test the performance of the DOT method on real tissue, we computed the orientation probabilities on data from an excised rat brain. A series of images were acquired at $17.6T$ using a Bruker Avance imaging system. Diffusion-weighted scans were acquired along 81 directions with a b-value of $1500s/mm^2$ along with a single image acquired at b ≈ 0. Resolution of the images were $150 \times 150 \times 300\mu m^3$.

For visualization purposes, we have overlaid the orientation surfaces on generalized anisotropy (GA) maps [10] computed from the displacement probabilities. The directionality of the probability profiles on the image plane is readily available from the surfaces. In order to visualize the peakedness through the image plane, we color coded the surface so that as the orientation of the surface varies from $-z$-axis to $+z$-axis, its color changes from blue to green. A selected slice from the three-dimensional data set is presented in Fig. 2. Although it was not possible to get meaningful orientation information from the apparent diffusivity profiles, the DOT method was able to clearly resolve the complex architecture of the rat medulla.

5. DISCUSSION AND CONCLUSION

An alternative form of the DOT technique was presented. Unlike the initial formulation, the presented reconstruction does not yield probabilities in terms of spherical harmonics. Instead, direct computation of probabilities along many direc-

Table 1. The angle between the computed and true fiber orientations (deviation angles) in degrees. Second column presents the deviation angle of each fiber when the DOT of noiseless signal profile is taken. Columns 3-6 show the mean and standard deviation values for the deviation angle when Gaussian noise of standard deviation 0.02 to 0.08 (from left to right) was added to the signal profiles. The computations for the DOT of noisy signals were repeated 100 times.

	$\psi\,(\sigma=0)$	$\psi\,(\sigma=0.02)$	$\psi\,(\sigma=0.04)$	$\psi\,(\sigma=0.06)$	$\psi\,(\sigma=0.08)$
1 fiber	$\{0.364\}$	0.77 ± 0.42	1.44 ± 0.79	2.20 ± 1.09	3.08 ± 1.66
2 fibers	$\{1.43, 0.80\}$	2.33 ± 1.10	3.66 ± 2.01	6.00 ± 5.57	8.07 ± 7.92
3 fibers	$\{2.87, 0.60, 4.57\}$	5.81 ± 5.84	11.5 ± 10.1	14.7 ± 10.3	17.6 ± 11.9

tions is possible via the nonparametric formulation. A matrix formulation of this method was presented that simplifies the implementation of the transform. Depending on the number of directions along which the probability values are desired, the nonparametric reconstruction scheme typically requires more memory to store the probability profiles. The simulation results demonstrated the accuracy of the estimated fiber orientations and its robustness to the noise levels. The experimental results further demonstrated the performance of the approach in real neural tissue.

Appendix

The following expressions define $\beta(\mathbf{u})$, $A_l(\mathbf{u})$ and $B_l(\mathbf{u})$ functions used above:

$$\beta(\mathbf{u}) = \frac{R_0}{\sqrt{D(\mathbf{u})\,t}} \; . \qquad (13)$$

$$A_l(\mathbf{u}) = \sum_{n=0}^{l/2} A_{ln}\,\beta(\mathbf{u})^{-2n} \text{ and } B_l(\mathbf{u}) = \sum_{n=0}^{l/2-1} B_{ln}\,\beta(\mathbf{u})^{-2n} \; . \qquad (14)$$

Here A_{ln} coefficients are given by

$$A_{ln} = \begin{cases} A^0 & , \text{if } n < 2 \\ A^0 + \sum_{t=1}^{n-1} A_{lnt} & , \text{if } n \geq 2 \end{cases} \qquad (15)$$

where

$$A^0 = \frac{(-1)^{l/2+n}}{n!}\,2^{2n}\left(\frac{l}{2}\right)_n\left(-\frac{l}{2}-\frac{1}{2}\right)_n , \qquad (16)$$

and

$$A_{lnt} = \frac{(2t-3)!!\left(\frac{l+3}{2}\right)_{n-t-1}\left(1-\frac{l}{2}\right)_{n-t-1}(l+1)!!}{(-1)^{t-1}\Gamma(l/2)(n-t-1)!\,2^{l/2-2n+t}} \; . \qquad (17)$$

Finally the B_{ln} coefficients are given by

$$B_{ln} = \frac{\left(\frac{l+3}{2}\right)_n\left(1-\frac{l}{2}\right)_n(l+1)!!}{\Gamma\left(\frac{l}{2}\right)n!\,2^{l/2-1-2n}} \; . \qquad (18)$$

Note that in the above definitions, $(l+1)!! = (l+1)(l-1)\cdots 1$ and $(a)_k$ is the Pochhammer symbol given by $(a)_k = a(a+1)(a+2)\cdots(a+k-1)$ with $(a)_0 = 1$.

6. REFERENCES

[1] P. J. Basser, J. Mattiello, and D. LeBihan, "Estimation of the effective self-diffusion tensor from the NMR spin echo," *J Magn Reson B*, vol. 103, no. 3, pp. 247–254, 1994.

[2] P. J. Basser, J. Mattiello, and D. LeBihan, "MR diffusion tensor spectroscopy and imaging," *Biophys J*, vol. 66, no. 1, pp. 259–267, 1994.

[3] E. O. Stejskal and J. E. Tanner, "Spin diffusion measurements: Spin echoes in the presence of a time-dependent field gradient," *J Chem Phys*, vol. 42, no. 1, pp. 288–292, 1965.

[4] P. T. Callaghan, *Principles of Nuclear Magnetic Resonance Microscopy*, Clarendon Press, Oxford, 1991.

[5] P. J. Basser, "Relationships between diffusion tensor and q-space MRI," *Magn Reson Med*, vol. 47, pp. 392–397, 2002.

[6] D. S. Tuch, R. M. Weisskoff, J. W. Belliveau, and V. J. Wedeen, "High angular resolution diffusion imaging of the human brain," in *Proc. of the 7th Annual Meeting of ISMRM, Philadelphia*, 1999, p. 321.

[7] E. Özarslan, T. M. Shepherd, B. C. Vemuri, S. J. Blackband, and T. H. Mareci, "Fast orientation mapping from HARDI," *LNCS*, vol. 3749-I, pp. 156–163, 2005.

[8] J. D. Jackson, *Classical Electrodynamics*, John Wiley & Sons, Inc, New York, 1999.

[9] O. Söderman and B. Jönsson, "Restricted diffusion in cylindirical geometry," *J Magn Reson*, vol. A, no. 117, pp. 94–97, 1995.

[10] E. Özarslan, B. C. Vemuri, and T. H. Mareci, "Generalized scalar measures for diffusion MRI using trace, variance and entropy," *Magn Reson Med*, vol. 53, no. 4, pp. 866–876, 2005.